Applied Catalysis A: General 353 (2009) 288–295

Reoxidation dynamics of highly dispersed VO_x species supported on γ-alumina

B. Frank[a,b], R. Fortrie[c,d], C. Hess[b,e], R. Schlögl[b], R. Schomäcker[a*]

[a]Department of Chemistry, Technical University of Berlin, Straße des 17. Juni 124, D-10623 Berlin, Germany
[b]Department of Inorganic Chemistry, Fritz Haber Institute of the Max Planck Society, Faradayweg 4-6, D-14195 Berlin, Germany
[c]Department of Chemistry, Humboldt University of Berlin, Unter den Linden 6, D-10099 Berlin, Germany
[d]Institut des Sciences Moléculaires de Marseille, Université Paul Cézanne et Ecole Centrale de Marseille, Case A62, Avenue Normandie-Niémen, 13397 Marseille Cedex 20, France
[e]Eduard-Zintl-Institute of Inorganic and Physical Chemistry, Darmstadt University of Technology, Petersenstr. 20, D-64287 Darmstadt, Germany

[*] Corresponding author: e-mail schomaecker@tu-berlin.de, Fax: +49 30 31421595

Received 9 July 2008, Received in revised form 10 October 2008, Accepted 5 November 2008, Available online 12 November 2008

Abstract

The $VO_x/\gamma\text{-}Al_2O_3$ catalyst VA-200, which was introduced in a previous article, is further characterized by XPS and visible Raman spectroscopy. The reoxidation of highly dispersed VO_x species with gas phase oxygen is investigated in detail and is described by an empirical kinetic model. It is observed that the reoxidation of reduced $VO_x/\gamma\text{-}Al_2O_3$ catalyst is strongly affected by the presence of water. The proposed kinetic model includes a distinct coverage of VO_x species with water or hydroxyl groups in the investigated temperature range of 479–712 K. Hydrated surface species are oxidized under release of water. Best fits of the experimental data can be achieved with first order rate laws with respect to oxygen concentration. Experiments are performed in an ideally mixed Berty-type reactor using oxygen step-marking over the reduced catalyst. The evolution of oxygen concentration using the kinetic model is in agreement with the experimentally observed behavior. The signal of water released during the reaction can be modeled only qualitatively, which (presumably) stems from its sorption behavior on the acidic alumina support. The oxidation of VO_x species furthermore depends on the reaction temperature. The oxidation of V^{+III} to V^{+V} cannot be completely achieved at temperatures below 673 K. However, the activation energy of this reaction is low, as suggested by the absence of strong variations of the response shapes with respect to temperature.

Keywords: $VO_x/\gamma\text{-}Al_2O_3$; vanadia; oxidation; kinetics; Mars-van Krevelen; water

1. Introduction

Development and optimization of supported vanadium oxide catalysts have attracted attention because of their activity in several partial oxidation and oxidative dehydrogenation reactions of saturated hydrocarbons [1-3]. These reactions are attractive alternatives towards present processes of olefin production. However, only a few processes have reached industrial application because of the poor selectivity due to consecutive oxidation of the reaction products [4-5].

The catalytic activity of vanadia is attributed to its reducible nature and its ability to easily change its oxidation state from V^{+III} up to V^{+V}. It is strongly influenced by the support material and the vanadia loading [6-8]. The

catalytic oxidation obeys the two-step kinetic model developed by Mars and van Krevelen (MvK) [9]. In the first step, the substrate reacts with some lattice oxygen atoms of the supported vanadia catalyst, which is reduced in the process. (The authors are aware of the fact that the MvK mechanism and related terms were developed for V_2O_5 bulk phase catalysts. However, in conformity with mechanistic aspects and the custom use in literature, the term "lattice oxygen" is used also for vanadyl and bridging oxygen atoms of dispersed non-crystalline VO_x species). The nature of the oxygen atom that is involved in the reaction is still under discussion. Bridging [2,10-12] or vanadyl oxygen atoms [13,14] have been proposed to be the active atom in the oxidation reaction, whereas computational studies have shown that vanadyl oxygen atoms are involved in the rate-determining step [15]. In both situations, one or more oxygen atoms are removed from the lattice. Vacancies are then consecutively filled by reaction with gas phase dioxygen molecules in the second step and the catalyst is reoxidized. In the present work it is considered that substrate oxidation and catalyst reoxidation are two independent steps. Many mechanistic studies covered the substrate conversion part whereas only a few studies on the reoxidation process can be found [16-18]. This may partly be due to the ratio of the absolute rates of both parts of the catalytic cycle. Reoxidation is much faster than substrate conversion in general which complicates its investigation by conventional steady state experiments. When reoxidation is not the rate determining step of the overall reaction, the reaction order for oxygen in formal kinetic approaches is low [19-23]. However, the analysis of the reoxidation step is of a fundamental interest.

Several investigations of the reoxidation of vanadium oxides and vanadia catalysts have been achieved using the temporal analysis of products (TAP) method [16-24], or analysis of transformations of ideal crystal surfaces either spectroscopically [25-28] or theoretically [29,30]. The experimental techniques require idealized ultra-high vacuum and/or clean monocrystal surfaces conditions, which can render the results problematic and contradictory [31]. These differences are well known and denoted with the term “pressure and materials gap”, which has to be negotiated when comparing the results gained from ideal and real systems. With that respect, a recent theoretical study combining DFT and Monte Carlo simulations brought new valuable information concerning the equilibrium structure of alumina supported vanadium oxides [50], but dynamic studies remain challenging.

Water plays an important role in partial oxidation reactions as it is a common product of selective oxidation reactions. Also, water vapor is often added to the feed to improve the catalyst performance. Previously is has been shown for vanadium containing catalysts that the presence of steam can significantly reduce the barrier for propane activation and/or shift the product spectrum from propylene to acrylic acid [32-34]. From a fundamental point of view, this raises questions about the value of the sticking coefficient of water on the catalyst surface at elevated temperatures.

In several studies on the microkinetics of the oxidative dehydrogenation of propane (ODP) at ambient conditions, the rates within the Mars-van Krevelen mechanism are modeled with 0.5^{th} and 1^{st} orders for oxygen and reduced vanadia sites, respectively [20,35,36]. Because reoxidation is fast compared to substrate conversion, these reaction orders were not determined experimentally but were based on schematic mechanistic considerations. However, 1^{st} rate order for oxygen partial pressure gives also reasonable fitting results [11,37,38].

Stated models for reoxidation predict simple reaction schemes including one or two elementary steps. However, these models were assumed for ambient experimental conditions, or gained from investigations under idealized conditions (TAP). Up to now, no experimental approach confirms these assumptions under “non-ideal” conditions. The Berty-type reactor is a powerful tool for the investigation of the reoxidation step under ambient conditions. Isothermic conditions and ideally-mixed gas phase combined with tracer step experiments allow new insights into this elementary reaction step in vanadia catalyzed oxidation reactions.

Among several differently supported VO_x catalysts prepared under comparable conditions the alumina supported sample showed the best catalytic performance in ODP with respect to propene selectivity [39]. The VO_x/γ-Al_2O_3 catalyst VA-200, introduced in a recent article [19], was thereby chosen for this study, however, a similar investigation is projected for low loaded SiO_2 (SBA-15) supported vanadium oxide samples [40].

2. Experimental

2.1. Catalyst preparation and characterization.

Low loaded VO_x/Al_2O_3 catalyst grains were prepared by wet saturation-impregnation of a commercial porous γ-alumina support with vanadyl acetylacetonate in toluenic solution. The method is described in a recent publication containing also fundamental characterization and catalytic performance in the oxidative dehydrogenation of propane (ODP) [19]. The characterization techniques, namely N_2-physisorption, X-ray diffraction (XRD), inductively coupled plasma spectroscopy (ICP-OES), UV-vis diffuse reflectance spectroscopy (UV-vis DRS), temperature programmed reduction (TPR), and O_2-titration, are described there. The resulting physico-chemical characteristics gained from the application of these methods and from additional characterization by Raman spectroscopy and X-ray photoelectron spectroscopy (XPS) are assembled in Tab. 1.

Table 1: Physico-chemical data of the low loaded VO_x/Al_2O_3 catalyst.

Property	Method	Result
BET surface area	N_2-physisorption	106.6 $m^2\ g^{-1}$
Average pore diameter	N_2-physisorption	15.7 nm
Phase composition	XRD	γ-Al_2O_3
Chemical composition	ICP-OES	1.4 wt.-% V
Surface composition (atomic ratio)	XPS	O: 61.2%, V: 2.5%, C: 3.8%, Al: 32.5%
Vanadia surface concentration	O_2-titration	1.55 V atoms nm^{-2}
State of vanadia species	TPR, UV-vis DRS, Raman spectroscopy	highly dispersed

In our previous study [19], oxygen titration of all vanadia species quantified by ICP was conducted at 773 K to test and confirm their accessibility for reaction with gas phase reactants. The present study implies a characterization of the redox-behaviour by varying the reoxidation temperature between 479 and 713 K. Further characterization of the vanadia species and their distribution is performed using XPS and Raman spectroscopy (see supplementary material).

2.2. Catalytic experiments in a Berty-type reactor.

Catalytic experiments were performed in a Berty "Micro" reactor purchased from Autoclave Engineers®. This internal cycle reactor is designed with a fixed, circular, and screened catalyst bed and a top mounted vane type blower. Gas circulation is directed downward along the vessel wall and deflected upward through the catalyst bed. The basket volume and the free vessel volume are 3.6 and 15.4 cm^3, respectively. The model used in this study is made of inert HASTELLOY® C-276 and designed for temperatures up to 800 K at a pressure of 345 bar. Ideal mixing conditions inside the vessel were proven by tracer step experiments switching the feed between N_2 and O_2. For this purpose the catalyst basket was filled with inert alumina grains with particle sizes similar to that of the catalyst (100–300 μm). The resulting concentration profiles for ambient conditions were detected by on-line mass spectrometry (MS) as shown in Fig. 1. A rotation speed of at least 4000 min^{-1} is required for ideal gas phase mixing for flow rates up to 100 $mL_n\ min^{-1}$, below this value a weak bypass flow can be observed. The ideally mixed reactor volume determined this way is in the range of 13 ± 0.5 mL, which is in good agreement with the data given by the supplier.

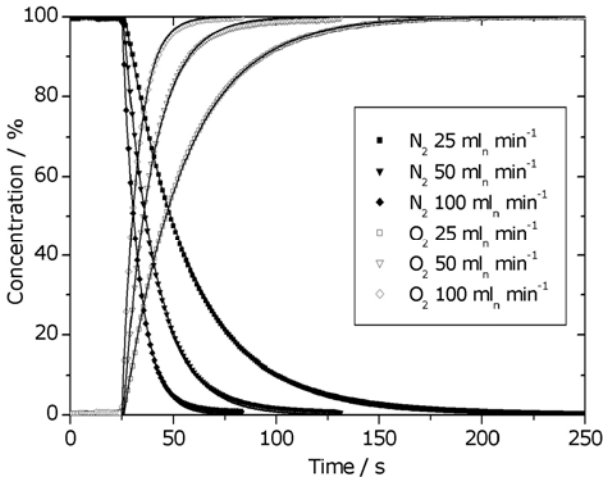

Fig. 1: Residence-time distribution of the Berty reactor from tracer step experiments switching the feed from nitrogen to oxygen at different flow rates; fit of the data with exponential decay functions (full lines).

The signal functions represent nearly ideal exponential decays indicating a well mixed gas phase inside the vessel. The signal curves can also be used to quantify the deviations from exponential decay functions which may be caused by back-mixing in tubing, particle filter and valves of the experimental set-up. As can be seen, their influence on the overall residence time behavior is negligible. During catalytic measurements the reactants were detected by on-line MS using a GAM 200 (InProcess Instruments) apparatus. Mass numbers of 2, 4, 14, 18, and 32 were monitored for the quantification of H_2, He, N_2, H_2O, and O_2, respectively, with a time resolution of 1.0 s.

For catalytic measurements the catalyst basket was filled with 1.0 g freshly calcined catalyst diluted with inert alumina particles of the same size and placed between two layers of this inert material. Reduction was achieved with 50 $mL_n\ min^{-1}$ of a H_2/N_2 mixture (20% H_2) at 713 K, changing the gas supply to pure hydrogen as water concen-

tration in the product flow began to decrease. After 30 min, the feed was switched to 50 $mL_n\ min^{-1}$ He for 1 h to flush the reactor and remove gas phase impurities of hydrogen and water at 713 K. This procedure was repeated strictly before each oxidation experiment to obtain a reproducible starting point. Afterwards, the reactor was cooled down to the required reaction temperature. As soon as the required temperature was reached, the He flow was increased to 100 $mL_n\ min^{-1}$ for 1 min, and the feed was switched to a 100 $mL_n\ min^{-1}$ flow of a O_2/N_2 mixture (3–10% O_2) to initiate the catalyst reoxidation. Similar experiments were repeated with an empty reactor set-up as well as loaded with pure γ-alumina grains at 713 K. Neither oxygen uptake nor water release were observed in these experiments indicating that detected transient responses of catalytic experiments are solely influenced by the interaction of oxygen with surface vanadia species. The reproducibility of the experiments is sufficient and confirms the suitability of the experimental set-up for dynamic experiments as well as the total reversibility of the redox cycles.

The modeling of catalytic experiments was performed with the "Berkeley Madonna" software [41] using a 4th order Runge-Kutta algorithm and experimental data fitting by the method of least square error.

3. Results and Discussion

3.1. Catalyst characterization.

Atomic ratios (%) of detected elements at the catalyst surface that were obtained from the XPS analysis are given in Tab. 1. The XP spectrum of the V $2p_{3/2}$ region after subtraction of X-ray induced satellites of the O 1s peak is shown in the supplementary material. The analysis shows that 80% V^{+V} and 20% V^{+IV} are present at $t = 0$ min. The resulting average oxidation degree of +4.8 is in agreement with incomplete oxidation of this catalyst sample at < 625 K as tested by oxygen titration experiments (E.V. Kondratenko, unpublished results) and as described below (Fig. 7).

The partial reduction can be explained by catalyst aging, e.g., the adsorption of water molecules from the ambient as observed recently for silica SBA-15 supported vanadium oxide catalysts [42-44]. Another explanation is the formation of stable polyvanadate species [45] which might be kinetically hindered from achieving a mean oxidation state of V^{+V} due to structural rearrangements being necessary, e.g.:

$$[V_3O_8]^{3-} + 0.5\ O_2 + 6\ OH^- \rightarrow 3\ [VO_4]^{3-} + 3\ H_2O$$

Structural rearrangements of surface vanadium oxide species (in the following denoted as VO_x) requiring mobility on the alumina surface are enabled by a low Tamman temperature of vanadia (482 K). Note however, that DFT calculations on protonated and silica supported VO_x clusters [15,18] cannot directly support this interpretation. The reduction of isolated V^{+V} sites by gas phase water molecules, which corresponds to the inverse of reactions 9–11 (release of ½ O_2, see below), is indeed strongly thermodynamically hindered. An indirect action of ambient water molecules proceeding first via adsorption on the alumina support and consecutive action on V^{+V} sites has, however, not been theoretically considered, neither has been the transformation of polynuclear species. These may be acceptable explanations.

The Raman spectra of oxidized and reduced VO_x/γ-Al_2O_3 catalyst VA-200 as well as of the pure support material are presented in supplementary material and compared to the spectrum of crystalline V_2O_5. In agreement with TPR data [19] the Raman analysis confirms the high dispersion of vanadium oxide species on the VA-200 surface. Probably due to a lower Raman cross-section of V^{+III} species, the reduced catalyst sample provides no bands detectable in the range of 300–1200 cm^{-1} and the spectrum appears identical to that of the support material. The disappearance of peaks related to vanadyl stretching vibrations furthermore suggests that at least a significant fraction of the catalyst is reduced under the chosen reaction conditions.

3.2. Kinetic modeling of experimental results.

A typical response signal of catalyst reoxidation after initiating a step function of 100 $mL_n\ min^{-1}$ O_2/N_2 (3% O_2) at 479 K is shown in Fig. 2. Compared to the nitrogen signal, which describes an exponential curve, the oxygen concentration increases moderately due to the oxygen consumption for catalyst reoxidation. With proceeding reoxidation, the oxygen consumption decreases. This is accompanied with an increase of the oxygen concentration that finally approaches the oxygen feed level. A modeled oxygen signal for a tracer step without reaction is shown as reference.

The following characteristics are observed in the oxygen signal: there are (i) a short delay in oxygen appearance compared to nitrogen for about 3 s, which indicates an extremely fast reaction at the beginning of the reoxidation process (see also Fig. 6 (b)), (ii) a step in oxygen concentration increase at $t = 10$ s, (iii) a bend at 0.4 mol m^{-3} oxygen concentration, and (iv) a sudden stop of the reaction at $t = 100$ s reflected in a relatively fast increase of the oxygen concentration to the inlet value. The appearance of water released during the reoxidation shows that the catalyst surface is not dry, although the reactor has been flushed with He at 713 K for about one hour. Moreover, the well-structured shape of the signal indicates a significant role of water sorption processes on the reoxidation kinetics, since the water peaks at 20 and 125 s correlate with characteristics of the oxygen outlet signal. The water signal is detected in the ppm range and displayed in arbitrary units (a.u.). The sorption equilibrium on inert alumina reduces its intensity and maxima sharpness.

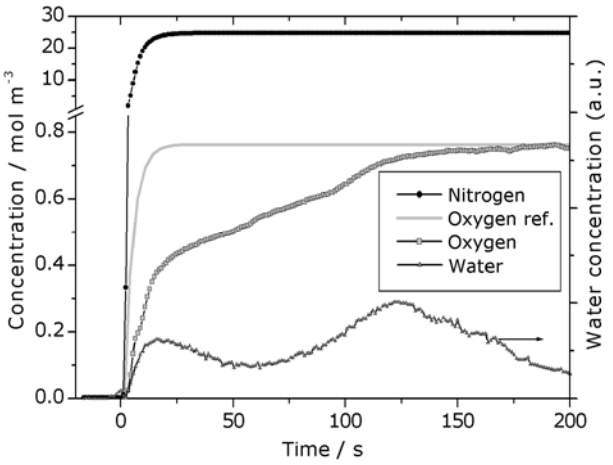

Fig. 2: Experimental response signal of VO_x/Al_2O_3 catalyst reoxidation; 100 mL_n min^{-1} O_2/N_2 (3% O_2), 479 K and 1 g catalyst containing 0.275 mmol V.

As a matter of fact, the detailed shape of the oxygen signal cannot be modeled using the simple reaction rate equations for catalyst reoxidation that are proposed in the literature. Previously, only the reaction of gas phase dioxygen molecules with V^{+III} sites was accounted for and the rate equations differed only in the reaction order of oxygen and vacancy concentrations. Then, the reoxidation of surface vanadia species was found to occur either directly in a dissociative mode [46] or by adsorption of molecular oxygen followed by dissociation [47]. Whereas the first mode is observed mainly in catalyst samples containing bulk vanadia phase, the latter kinetics can be ascribed to highly dispersed species, e.g. supported on silica [48]. The following reaction rate laws $r_i = dc([V^{+V}O])/dt$ for the formation of V^{+V} sites were derived for these mechanisms (Eqs. 1–3):

$$r_1 = k_1\, c(O_2)^{0.5}\, c([V^{+III}]) \quad (1)$$

$$r_2 = k_2\, c(O_2)\, c([V^{+III}])^2 \quad (2)$$

$$r_3 = k_3\, c(O_2)\, c([V^{+III}]) \quad (3)$$

These rate laws are ascribed to the reactions 4–6:

$$0.5\ O_2 + [V^{+III}] \rightarrow [V^{+V}O] \quad (4)$$

$$O_2 + 2\ [V^{+III}] \rightarrow 2\ [V^{+V}O] \quad (5)$$

$$O_2 + [V^{+III}] \rightarrow [V^{+V}O_2] \quad (6)$$

$$[V^{+V}O_2] + [V^{+III}] \rightarrow 2\ [V^{+V}O] \quad (7)$$

where reactions 4 and 5 correspond to rates r_1 and r_2, respectively [20]. In r_1, the rate of oxygen adsorption is relatively slow compared to its dissociation and *vice versa* in r_2; Reaction 6 describes molecular adsorption of oxygen with consecutive dissociation (reaction 7), as kinetically described in r_3 in case of adsorption being rate determining.

For better comparison of the curve shapes, the oxygen signal at the outlet of the Berty reactor was modeled using these relatively simple models. The result is shown in Fig. 3 for an oxygen concentration of 0.76 mol m^{-3} (3 vol.-% O_2) at 479 K. The response shapes of the signals are normalized by adjustment of rate constants k_i with respect to the bend of the curve after the initial increase of the oxygen concentrations from t = 0–10 s (see arrow in Fig. 3) to allow a better comparison. When oxygen concentration is ca. 0.4 mol m^{-3} at t = 10 s, a bend reflects the beginning of the reoxidation process, since oxygen concentration is too low for remarkable conversion at t < 10 s. The resulting response curves are similar for the chosen modeling conditions. However, they strongly differ when oxygen concentration, flow rate, or total number of active sites varies because of the different reactant reaction orders.

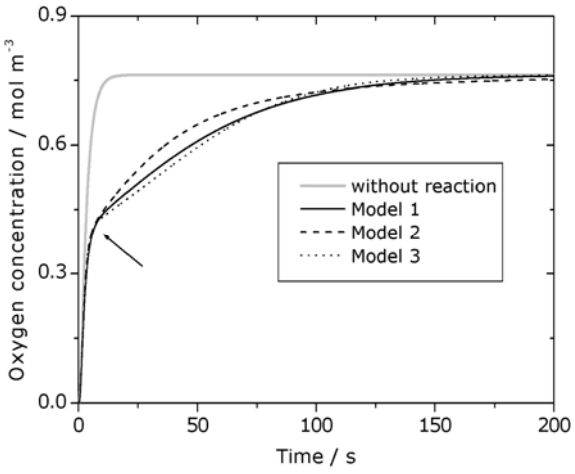

Fig. 3: Simulation of the oxygen signals at the outlet of the reactor during the catalyst reoxidation process by models presented in the literature (model 1–3 correspond to Eqs. 1–3, respectively); arbitrary rate constants.

A simulated oxygen response curve without reaction is given as reference. The oxygen concentration calculated using the reoxidation models is below this curve for the whole simulation due to the oxygen consumption in the reactor. The total amount of oxygen required for catalyst reoxidation is given by the area between the two curves and is identical for models 1–3.

As could be shown, an accurate modeling of the reoxidation dynamics cannot succeed without considering the interaction of water as co-reactant. This is all the more obligatory as this compound is the side product of oxidative dehydrogenations and thereby always present in the reaction gas mixture. However, taking sorption processes of water as well as the mobility of hydrogen, oxygen, hydroxyls or water molecules on the catalyst surface into account, a huge number of reaction steps arises even when making

Table 2: Selected reaction steps between surface vanadia species and gas phase oxygen and water or adsorbed oxygen, hydrogen, and hydroxyls on alumina surface of $VO_x/\gamma\text{-}Al_2O_3$ catalyst.

		gas phase / adsorbed species converted by reaction with surface vanadia site (arrow points at resulting species)				
No.	surface species[a]	O_2(g)	H_2O(g)	OH(ads)	O(ads)	H(ads)
1	$[V^{+III}]$	→ ***5*** [b]	→ ***4***	→ ***3***	→ ***2***	-
2	$[V^{+V}O]$	-	→ ***7***	→ ***6***	→ ***5***	→ ***3***
3	$[V^{+IV}OH]$	→ ***9***	→ ***8***	→ ***7***	→ ***6***	→ ***4***
4	$[V^{+III}OH_2]$	→ ***10***	-	→ ***8***	→ ***7***	-
5	$[V^{+V}O_2]$	-	→ ***10***	→ ***9***	-	→ ***6***
6	$[V^{+IV/+V}(O)OH]$	-	-	→ ***10***	→ ***9***	→ ***7***
7	$[V^{+V}(OH)_2]$	-	-	-	→ ***10***	→ ***8***
8	$[V^{+IV}(OH)(OH_2)]$	-	-	-	-	-
9	$[V^{+V}(O_2)(OH)]$	-	-	-	-	→ ***10***
10	$[V^{+IV/+V}(O_2)(OH_2)]$	-	-	-	-	-

some substantial simplifications, i.e., all vanadia species being (i) monomeric (absence of bridging V-O-V bonds), (ii) triply bonded to the surface by three V-O-Al bonds, and (iii) not directly bonded to hydrogen atoms. Taking these assumptions into account, a selection of 25 theoretically possible reaction steps is assembled in Tab. 2.

In the following it will be shown that complex transient responses experimentally derived can be modeled using a selection of reaction steps from Tab. 2. Due to severe simplifications and with regard to the enormous number of constants to be fitted a physical meaning of the derived reaction scheme must be regarded with caution and fitted kinetic constants have no physical meaning, actually not until the reaction scheme has been confirmed by independent methods, i.e. spectroscopy or theory.

For model discrimination, in addition to reactions 4-7, the following reactions are chosen and give sufficient fitting result:

$$H_2O + [V^{+III}] \rightarrow [V^{+III}OH_2] \quad (8)$$

$$0.5\ O_2 + [V^{+III}OH_2] \rightarrow [V^{+V}(OH)_2] \quad (9)$$

$$[V^{+V}(OH)_2] \rightarrow [V^{+V}O(OH_2)] \quad (10)$$

$$[V^{+V}O(OH_2)] \rightarrow [V^{+V}O] + H_2O \quad (11)$$

$$[V^{+III}OH_2] + [V^{+V}O] \rightarrow 2\ [V^{+IV}OH] \quad (12)$$

$$0.5\ O_2 + [V^{+IV}OH] \rightarrow [V^{+V}O(OH)] \quad (13)$$

$$[V^{+V}O(OH)] + [V^{+IV}OH] \rightarrow [V^{+V}O(OH_2)] + [V^{+V}O] \quad (14)$$

$$H_2O + [Al_2O_3] \rightarrow [Al_2O_3OH_2] \quad (15)$$

where [V] stands for a structurally undefined surface vanadia species as active site and $[Al_2O_3]$ for a γ-alumina surface site. It has to be stressed that this set of reactions does not represent a complete set of possible elementary reactions, neither are most of these steps elementary reactions at all. Although sorption steps 8 and 11 may be regarded as elementary and possibly also reaction 10, which states an intramolecular rearrangement, other steps imply the mobility of hydrogen atoms on the alumina surface (Eqs. 12 and 14) or the dissociation of dioxygen (Eqs. 9 and 13). However, the chosen basis set of empirical reactions can provide important information about the reaction pathways during oxidation and thereby can be used as a basis for further investigation of real elementary reactions on a quantum chemical basis, which is project of future research.

The addition of a second type of active site, which allows for a differentiation between monomeric and dimeric/polymeric structures, was not found to improve the fitting of experimental data and is therefore avoided. However, a heterogeneous composition of vanadia species including vanadia monomers, dimers, and polymers cannot be excluded from spectroscopic analysis of the catalyst. The kinetic modeling, however, indicates a similar catalytic

behaviour of these species. Other structural differences between reduced and oxidized active sites are also not taken into account. It is worth mentioning that despite great afford the model described above (Eqs. 4, 8–14) is so far the only capable one for accurate fitting of experimental data, i.e. diminishing the number of possible reaction steps leads to a worsening of the agreement between model and experimental data.

However, the described model fails in quantitatively describing the complex response of water. This can be attributed to water sorption on alumina (Eq. 15) that could not be included successfully into the modeling. The modeled values, however, may approximate the intraparticle water concentration or a pseudo-concentration due to migration of mobile water molecules on the catalyst surface between vanadia and alumina sites. After leaving the catalyst particle, most of the water is assumed to adsorb irreversibly on the alumina grains, especially at temperatures below the reduction temperature. The resulting outlet concentration, however, is too low for accurate handling in the numerical integration process of microkinetic modeling and could thereby not be described.

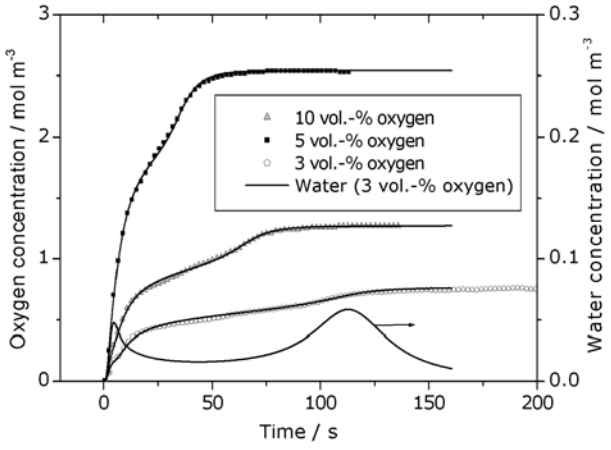

Fig. 4: Experimental results and simulated response curves of oxygen to step-marking with different oxygen concentrations at 479 K, water response for 3 vol.-% O_2.

The fit of the rate constants of these empirical reactions was performed in parallel on three datasets measured at 479 K and oxygen concentrations of 3, 5, and 10 vol.-%. The essential characteristics of the oxygen and water signals are reflected. However, the direct oxidation of naked V^{+III} to V^{+V} (Eq. 4) appears negligible compared to a reoxidation process via vanadia hydroxyls [$V^{+IV}OH$] and vanadia adsorbed water [$V^{+III}OH_2$] as intermediates. Moreover, a forced inclusion of direct oxidation reactions (Eqs. 4–7) with substantial contribution to the overall reaction resulted in a poor accuracy of the fit, which supports the negligible impact of the direct oxidation under oxidative dehydrogenation conditions. The calculated surface coverage with transition species [$V^{+V}(OH)_2$], [$V^{+V}O(OH_2)$], and [$V^{+V}O(OH)$] was found to be low ($\theta < 0.1\%$), which means also that their decomposition (Eqs. 10,11,14) is very fast and not rate determining for the overall reaction rate. Furthermore, the best fit was achieved with first order rate laws with respect to oxygen and surface species for the reactions including oxygen. This validates a consecutive adsorption-dissociation model as expected for the low loaded catalyst, and implies a peroxo species, which decomposes quickly, as precursor for the species [$V^{+V}(OH)_2$], [$V^{+V}O(OH_2)$], and [$V^{+V}O(OH)$] [18]. This drastically reduces the number of rate equations that are relevant in the description of the measured responses. The modeling suggests the reaction mechanism shown in Fig. 5.

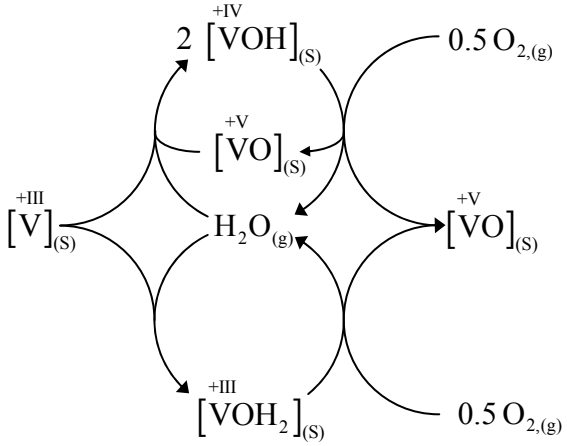

Fig. 5: Proposed reaction network of oxidation of highly dispersed hydrated VO_x species supported on γ-Al_2O_3.

Small amounts of water in the system adsorb predominantly on the V^{+III} sites (Eq. 10). It is concluded from the experiments that, compared to naked V^{+III} sites, these hydrated species react more easily with gas phase oxygen. Since water is only weakly adsorbed on V^{+V} sites, the reoxidation process finally results in the release of the adsorbed water (Eq. 11), which then adsorbs instantly on the next free V^{+III} active site. When a certain amount of V^{+V} sites is present at the surface, the reaction mechanism changes, and water adsorbs dissociatively on V^{+V} and V^{+III} sites to produce two hydroxylated V^{+IV} sites (Eq. 12). Hydroxyls are also a favorable point of attack for reoxidation compared to naked V^{+III} and get oxidized under release of water (Eq. 13). These consecutively occurring cycles are responsible for the sudden release of water and its batch-wise appearance in the reoxidation signal (Fig. 2). Since there is still some uncertainty about the absolute water concentration in particles and gas phase, the absolute values of the rate constants are not published here but in a supporting information file. Furthermore, water released during the reoxidation might not be released in the gas phase but migrate on the alumina surface. Consequently, the reverse pathway, which is the migration of mobile water molecules from hydrated alumina sites onto naked V^{+III} sites, should also be taken into account. The model described above is

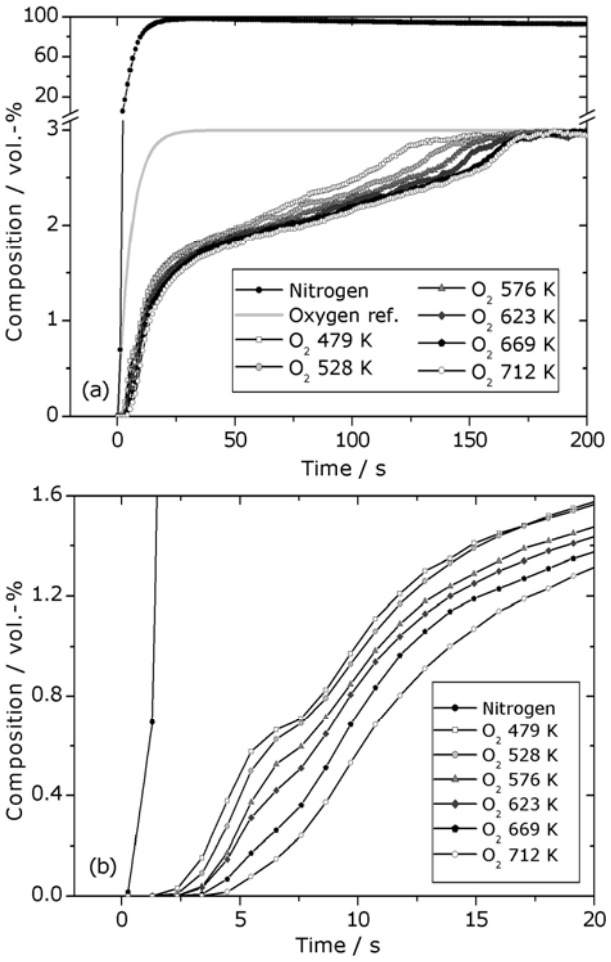

Fig. 6: Reoxidation responses to step-marking with 3 vol.-% O_2 in the temperature range of 479–712 K (a, 200 s), magnification of the initial period (b, 20 s).

confirmed by its capability to predict the reoxidation of partial reduced VO_x/Al_2O_3 catalyst (see supplementary information).

Given recently reported DFT data [18], a minor occupation of reduced sites with adsorbed water does not appear unreasonable with regard to uncertainties of the calculations. The calculated free energies of water adsorption on V^{+III} (Eq. 8) are -66, +31, and +65 kJ mol^{-1} at zero point, 600, and 800 K, respectively. Rozanska et al. also showed that reoxidation of $[V^{+IV}OH]$ sites by O_2 (Eq. 14) is possible with a low barrier and reoxidation of $[V^{+III}OH_2]$ sites by O_2 (Eq. 10) is possible without any apparent barrier. However, their calculations also show that reoxidation of water-free $[V^{+III}]$ sites leading to peroxo-intermediates is even more favourable [18].

To further investigate the impact of water on the reoxidation, several experiments were conducted with addition of steam to the gas mixture. The lowest concentration that could be adjusted using a conventional saturator is ca. 0.6 % (water saturation pressure at 274 K). However, even this concentration is too high and the detailed structures of both oxygen and water response curve disappear at temperatures lower than the reduction temperature. As expected, the reoxidation rate also becomes retarded. It can be concluded that in case of water being present in the feed, V^{+III} sites and γ-Al_2O_3 surface are immediately fully saturated with water that inhibits the reaction and leads to signal-smearing.

The influence of the reaction temperature on the reoxidation process was then investigated. The oxygen response curves at temperatures between 479 and 712 K is depicted in Fig. 6 (a). A feed containing 3 vol.-% oxygen was used. Fig. 6 (b) is an enlargement of the initial phase of the reoxidation. Again, the nitrogen curve can be used as reference for ideal residence-time distribution.

Two conclusions can be drawn from Fig. 6 (a): (i) the curve shapes are quite similar over a wide range of temperatures, which means that the activation energy of vanadia reoxidation occurring via water adsorption is relatively low, and (ii) the overall oxygen consumption increases with temperature.

The influence of temperature on the reaction steps of reoxidation can be observed in the initial phase of the reaction (Fig. 6 (b)). The shoulder in oxygen concentration at $t \approx 7$ s is relatively pronounced at low temperatures and absent at high temperatures with a fluent transition. The disappearance of this shoulder and the extension of the initial period where nearly no oxygen passes the reactor, is due to the acceleration of reaction 9. The impact of increasing temperature on reaction 13 results in a general decline of the oxygen concentration level in the range of 10 s up to the end of the reaction, respectively.

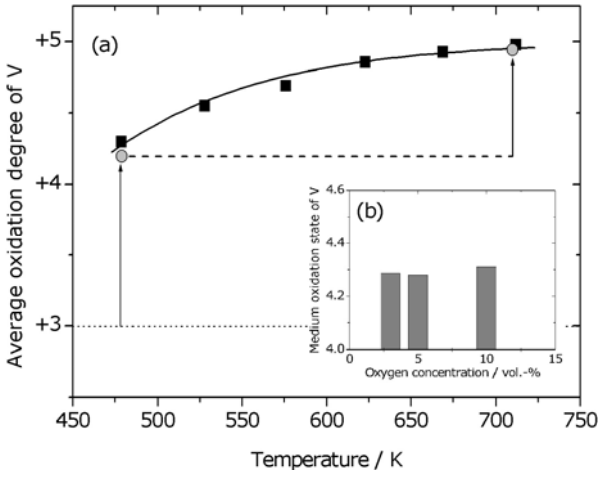

Fig. 7.: Final average oxidation degree of VO_x species on catalyst VA-200 after reoxidation experiments with 3 vol.-% O_2 gas mixture (a), variation of oxygen concentration at 479 K (b).

The oxygen consumption as a function of reoxidation temperature is displayed in Fig. 7 (a, full squares) and is referred to the total amount of vanadia in the reactor. The resulting oxidation state of vanadium is plotted. The maximum oxidation state of V^{+V} is approached at high temperatures, the maximum change in oxidation state being $\Delta = +2$. It can be concluded that the starting point of each reoxida

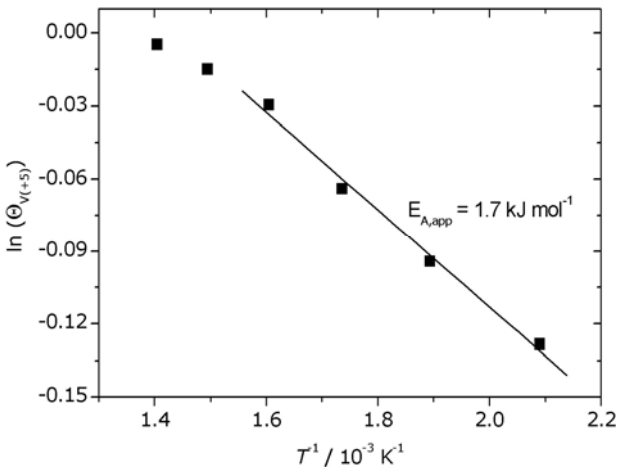

Fig. 8: Arrhenius-type plot of final V^{+V}-fraction after reoxidation.

tion experiment corresponds to a sample containing almost only V^{+III} species. However, the total oxygen consumption decreases below 700 K and the average change in oxidation state is only +1.3 (479 K).

Fig. 7 (b) shows that the inlet oxygen concentration has no impact on the amount of consumed oxygen during reoxidation at 479 K. This indicates that the incomplete reoxidation is a kinetic rather than a thermodynamic effect as discussed in the characterization section. The catalyst can also be reoxidized step-wise (Fig. 7 (a), grey circles). After partial oxidation of V^{+III} sites to an average oxidation degree of $V^{+4.3}$ at 479 K, the reactor was heated up to 709 K under helium. A continued oxidation resulted in the maximum oxidation state V^{+V}, which is also reached by total reoxidation in this temperature range. A lower number of V^{+V} active sites at lower temperatures can have an influence on the experimentally determined activation energy of each reaction that depends on the V^{+III}/V^{+V} redox cycle. This is not the case: to monitor this falsifying effect, which is observable up to about 623 K, the fraction of active sites V^{+V}/V_{tot} was plotted in an Arrhenius-type diagram (Fig. 8).

The slope in the range of 479–523 K gives a contribution to the apparent activation energy of 1.7 kJ mol^{-1}, caused solely by different fraction of V^{+V} sites. A falsifying impact in this order of magnitude is negligible especially for exothermic reactions. Above 523 K this contribution even decreases and approaches to zero at temperatures of about 773 K.

4. Conclusions

The reoxidation of highly dispersed VO_x species supported on a γ-Al_2O_3 surface is a very complex process and not as simple as reported in recent literature. For ODH reactions water is a key intermediate, whose presence can increase the overall rate of the reoxidation reaction. This was evidenced by transient experiments performed introducing oxygen into an ideally-mixed Berty-type reactor containing reduced VA-200 catalyst. The complex transient response to oxygen step-marking indicates a strong influence of adsorbed water remaining from the reduction using hydrogen. However, when water is added to the feed in higher concentrations, its inhibiting effect on the overall reaction is prevailing, and the details of the complex response curve disappear. It is thereby concluded, that only trace amounts of water can affect the reoxidation of surface VO_x species positively.

A microkinetic analysis of these response curves was aspired but determination of kinetic constants failed in the enormous number of elementary steps possible on the catalyst surface. One possibility for a reaction scheme derived from kinetic fit is presented but physical meaning is given not until the proposed scheme is confirmed either spectroscopically or theoretically. However, inclusion of water sorption processes on vanadia and alumina as well as the reactivity of hydrogen, oxygen, hydroxyls, and water molecules on the catalyst surface between vanadia and alumina sites was proven to be important for kinetic analysis and is projected for future researches. Regarding the relevancy of proposed reaction scheme as a part of MvK redox cycle in ODH reactions, it is worth mentioning, that the reduction of vanadia species with hydrogen yields V^{+III} species, whose appearance in oxidative dehydrogenations, depending on reaction conditions, is neither experimentally observed in each case, nor theoretically required. It is also possible that V^{+III} does not appear at all and that the reoxidation occurs directly on V^{+IV} species or species including the adsorbed substrate.

Furthermore the low loaded VO_x/γ-Al_2O_3 catalyst VA-200, introduced in our previous study [19], has been characterized by XPS and Raman spectroscopy, as well as by oxygen titration. These methods confirm the presence of dispersed VO_x species on the surface, which are all accessible for gas phase oxygen. The amount of oxygen consumed during one reoxidation experiment depends on the reaction temperature and corresponds to a change in the average oxidation degree of vanadia of $\Delta = +2$ at temperatures above 673 K. Below this temperature a smaller oxygen consumption indicates an incomplete oxidation, which could not be enhanced by variation of the oxygen concentration in the feed. If referred to a kinetic barrier this is not in contradiction to the theoretical calculations. They show that the oxidation of VO_x species is favored over the whole range of temperatures investigated and independent from water adsorption or hydroxylation. On the other hand a surface structure substantially different from that one used for DFT calculations may be present on the surface of VA-200, e.g., polymeric species as proposed recently [45,49] even for extremely low loaded VO_x/γ-Al_2O_3 and VO_x/SBA-15 catalysts.

Acknowledgement

This work was supported by the German Research Foundation (Deutsche Forschungsgemeinschaft, DFG) in the frame of the collaborative research center “Structure,

dynamics and reactivity of transition metal oxide aggregates" (Sonderforschungsbereich 546). C. Hess thanks the DFG for providing an Emmy Noether fellowship. The authors are furthermore grateful to E.V. Kondratenko for performing oxygen titration experiments, to X. Rozanska and J. Sauer for helpful comments on the manuscript.

References and Notes

[1] M.D. Argyle, K. Chen, A.T. Bell, E. Iglesia, J. Catal. 208 (2002) 139.
[2] I.E. Wachs, Catal. Today 100 (2005) 79.
[3] E.A. Mamedov, V. Cortés Corberán, Appl. Catal. A: Gen. 127 (1995) 1.
[4] M.M. Bhasin, J.H. McCain, B.V. Vora, T. Imai, P.R. Pujadó, Appl. Catal. A: Gen. 221 (2001) 397.
[5] F. Cavani, G. Centi, C. Perego, A. Vaccari A., Catal. Today 99 (2005) 1, and references therein.
[6] G. Martra, F. Arena, S. Coluccia, F. Frusteri, A. Parmaliana, Catal. Today 63 (2000) 197.
[7] F. Arena, F. Frusteri, A. Parmaliana, Catal. Lett. 60 (1999) 59.
[8] A.A. Lemonidou, L. Nalbandian, I.A. Vasalos, Catal. Today 61 (2000) 61.
[9] P. Mars, D.W. van Krevelen, Spec. Suppl. Chem. Eng. Sci. 3 (1954) 41.
[10] A. Khodakov, J. Yang, S. Su, E. Iglesia, A.T. Bell, J. Catal. 177 (1998) 343.
[11] K. Routray, K.R.S.K. Reddy, G. Deo, Appl. Catal. A: Gen. 265 (2004) 265.
[12] J.G. Eon, R. Olier, J.C. Volta, J. Catal. 145 (1994) 318.
[13] J. Le Bars, A. Auroux, M. Forissier, J.C. Vedrine, J. Catal. 162 (1996) 250.
[14] S.T. Oyama, J. Catal. 128 (1991) 210.
[15] X. Rozanska, R. Fortrie, J. Sauer, J. Phys. Chem. C 111 (2007) 6041.
[16] I. Sack, V. Balcaen, M. Olea, H. Poelman, G.B. Marin, Catal. Today 112 (2006) 68.
[17] J. Słoczyński, Appl. Catal. A: Gen. 146 (1996) 401.
[18] X. Rozanska, E.V. Kondratenko, J. Sauer, J. Catal. 256 (2008) 84.
[19] B. Frank, A. Dinse, O. Ovsitser, E.V. Kondratenko, R. Schomäcker, Appl. Catal. A: Gen. 323 (2007) 66.
[20] R. Grabowski, J. Słoczyñski, N.M. Grzesik, Appl. Catal. A: Gen. 242 (2003) 297.
[21] L. Låte, E.A. Blekkan, J. Nat. Gas Chem. 11 (2002) 33.
[22] D. Creaser, B. Andersson, Appl. Catal. A: Gen. 141 (1996) 131.
[23] A. Bottino, G. Capannelli, A. Comite, S. Storace, R. Di Felice, Chem. Eng. J. 94 (2003) 11.
[24] E.V. Kondratenko, O. Buyevskaya, M. Baerns, J. Mol. Catal. A: Chem. 158 (2000) 199.
[25] M. Abu Haija, S. Guimond, Y. Romanyshyn, A. Uhl, H. Kuhlenbeck, T.K. Todorova, M.V. Ganduglia-Pirovano, J. Döbler, J. Sauer, H.J. Freund, Surf. Sci. 600 (2006) 1040.
[26] M. Abu Haija, S. Guimond, A. Uhl, H. Kuhlenbeck, H.J. Freund, Surf. Sci. 600 (2006) 1497.
[27] A.C. Dupuis, M. Abu Haija, B. Richter, H. Kuhlenbeck, H.J. Freund, Surf. Sci. 539 (2003) 99.
[28] J. Schoiswohl, M. Sock, S. Surnev, M.G. Ramsey, F.P. Netzer, G. Kresse, J.N. Andersen, Surf. Sci. 555 (2004) 101.
[29] G. Kresse, S. Surnev, J. Schoiswohl, F.P. Netzer, Surf. Sci. 555 (2004) 118.
[30] I. Czekaj, K. Hermann, M. Witko, Surf. Sci. 545 (2003) 85.
[31] G.A. Somorjai, Surf. Sci. 299/300 (1994) 849.
[32] M.M. Lin, Appl. Catal. A: Gen. 207 (2001) 1.
[33] G. Lani, L. Lisi, J.C. Volta, Catal. Today 91-92 (2004) 275.
[34] C. Hess, M.H. Looi, S.B. Abd Hamid, R. Schlögl, Chem. Commun. 2006 451.
[35] R. Grabowski, Appl. Catal. A: Gen. 270 (2004) 37.
[36] R. Tesser, V. Maradei, M. Di Serio, E. Santacesaria, Ind. Eng. Chem. Res. 43 (2004) 1623.
[37] K. Chen, A. Khodakov, J. Yang, A.T. Bell, E. Iglesia, J. Catal. 186 (1999) 325.
[38] D. Wolf, N. Dropka, Q. Smejkal, O. Buyevskaya, Chem. Eng. Sci. 56 (2001) 713.
[39] A. Dinse, B. Frank, C. Hess, D. Habel, R. Schomäcker, J. Mol. Catal. A: Chem. 289 (2008) 28.
[40] C. Hess, J.D. Hoefelmeyer, T.D. Tilley, J. Phys. Chem. B 108 (2004) 9703.
[41] http://www.berkeleymadonna.com/
[42] C. Hess, R. Schlögl, Chem. Phys. Lett. 432 (2006) 139.
[43] C. Hess, G. Tzolova-Müller, R. Herbert, J. Phys. Chem. C 111 (2007) 9471.
[44] C. Hess, J. Catal. 248 (2007) 120.
[45] F. Klose, T. Wolff, H. Lorenz, A. Seidel-Morgenstern, Y. Suchorski, M. Piórkowska, H. Weiss, J. Catal. 247 (2007) 176.
[46] G.K. Boreskov, V.S. Muzykantov, Ann. N.Y. Acad. Sci. 213 (1973) 137.
[47] A. Pantazidis, S.A. Buchholz, H.W. Zanthoff, Y. Schuurman, C. Mirodatos, Catal. Today 40 (1998) 207.
[48] J.R. Anderson, M. Boudart, (Eds.) Catalysis Science and Technology, Vol. 3, Springer, Berlin, 1982.
[49] T.V. Venkov, C. Hess, F.C. Jentoft, Langmuir 23 (2007) 1768.
[50] R. Fortrie, T.K. Todorova, M.V. Ganduglia-Pirovano, J. Sauer, J. Chem. Phys (2008), submitted.